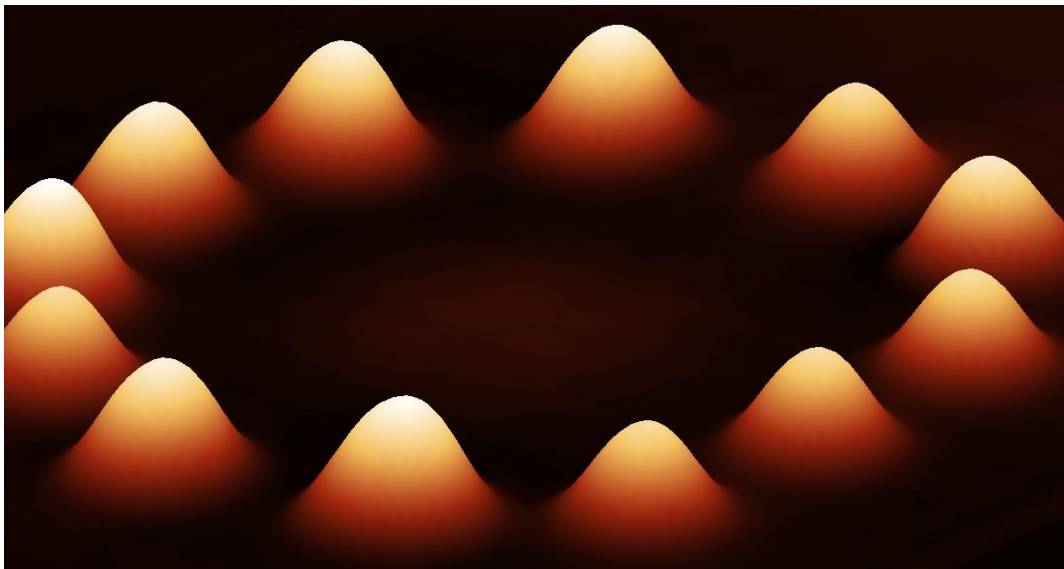**Universiteit Utrecht**

## Opleidingen Natuur- en Scheikunde

# Creating Quantum Corrals on Ag(111)/Si(111): Looking for increased Energy Resolution

BACHELOR THESIS

*Roel G.R. van Wijk*

*Supervisors*:

Rian A.M. LIGTHART MSc
Debye Institute for Nanomaterials Science

Dr. Ingmar SWART
Debye Institute for Nanomaterials Science

2 July 2021

**Abstract**

By means of atomic manipulation the Scanning Tunnelling Microscope (STM) can be used to build electronic quantum simulators. Previous work has proved CO on Cu(111) to be a reliable system for this. However, energy broadening due to coupling of the surface state with bulk states, poses a problem for the CO/Cu(111) system. In this thesis, thin Ag(111) films on Si(111) are examined as coupling with bulk states is impossible in the silicon band gap. It is shown that, by using an STM, manipulation of Ag adatoms is possible through which two quantum corrals and a dimer were realised. By fitting Gaussian functions to peaks in differential conductance spectra, the energy broadening was determined in terms of Full Width at Half Maximum (FWHM) values. Furthermore, muffin-tin calculations were performed and are compared to experimental observations. In the quantum corrals, $1s$-like, $1p$-like and $2s$-like states were observed from analysing differential conductance spectra. In the dimer $1s$-like and $1p$-like bonding and anti-bonding states were observed. FWHM values are compared to that of quantum corrals on a CO/Cu(111) system from a previous study. Although direct comparison is not possible, FWHM values found on the Ag(111)/Si(111) system are in the order of tens of millivolts smaller than on the CO/Cu(111) system. Still, it is questioned whether bulk states were present or not due to a too thick Ag layer, having resulted in more energy broadening than expected. Overall, this thesis contributes to the search for electronic quantum simulators with higher energy resolution.

**Front page:** Three-dimensional representation of a constant current image made with a scanning tunnelling microscope showing a quantum corral. The corral was created by controlled positioning of Ag small atomic clusters on the surface of a Si(111) wafer covered with Ag(111). The diameter of the corral is approximately 6.4 nanometres.

i

# Contents

# 1   Introduction

Quantum mechanical theories have helped to understand many phenomena observed in experiments. Certain quantum systems that are difficult to study in the laboratory or model with a supercomputer can be studied in so-called quantum simulators. Quantum simulators include ultracold quantum gasses, trapped ions, quantum dots, photonic systems and electronic lattices [1]. The invention of the Scanning Tunnelling Microscope (STM) in 1981 [2], which was granted a Nobel Prize in 1986 [3], paved the way for the creation of the quantum simulator based on electrons. The STM enables the controlled positioning of single atoms on a surface. By doing so, two-dimensional electronic lattices can be created at will to simulate real electronic materials [4]. Electronic lattices have been built using CO on Cu(111) [5–9], Cl on Cu(100) [10], Ag on Ag(111) [11] or Mn on Ag(111) [12]. Working with the CO on Cu(111) system is favoured due to the reliability of CO manipulation [5, 13].

On electronic lattices the Local Density Of States (LDOS) is measured to learn about the electronic states. In case of the CO on Cu(111) system, LDOS measurements exhibit a Lorentzian energy broadening of approximately 80 meV [5]. The broadening is mainly caused by enhanced coupling between surface and bulk states via CO molecules [5]. Broadening in LDOS measurements can make it difficult, if not impossible, to distinguish electronic states which are close to each other in energy. Thus, there is a need for novel systems which limit the coupling between surface and bulk states and thereby increase the energy resolution.

To attain higher energy resolution, a system made of Si(111) coated with a thin layer[1] of Ag(111), is a candidate. Ag(111) has a free surface state onset at -70 mV [14] and would thus live inside the 1.17 eV[2] [15] band gap of the intrinsic semiconductor Si(111). Hence, there will be no bulk states (in the band gap) for the surface state to couple with and consequently less energy broadening. In addition, Sawa *et al.* [16] reported that the free surface state offset of thin Ag(111) films on Si(111) go up in energy with decreasing film thickness. Nonetheless, the surface state offset will remain inside the silicon band gap.

In order to be able to test the energy resolution on the Ag(111)/Si(111) system, effective manipulation of atoms on the surface is a prerequisite. Previous studies show that manipulation of Ag adatoms on bulk Ag(111) is possible [11, 17]. It has also been demonstrated that atoms can be pulled out of the Ag(111) substrate and placed on the surface [18]. However, no previous work has shown that these manipulations also work on Ag(111)/Si(111) systems.

In this thesis Ag(111)/Si(111) is tested on the energy resolution it yields. To that end, two Si(111) samples were coated with a different amount of Ag layers. An STM was used to build quantum corrals and dimers of which the LDOS was measured. Peaks in these spectra were attributed to electronic states analogous to hydrogen atomic orbitals. The widths of peaks were determined and compared.

---

[1]In the order of five to ten monolayers.
[2]For sub 100 K temperatures.

# 2   Theory

This chapter offers the theoretical background needed in order to understand the conducted experiments and the interpretations thereof. Firstly, the STM is introduced and three of its important features are explained in the following order: imaging, scanning tunnelling spectroscopy, and atom manipulation. Consequently quantum corrals are clarified. Finally, features of the Ag(111)/Si(111) samples used in the experiment, are discussed.

## 2.1   Scanning Tunnelling Microscopy

The STM can be used to image sample surfaces with atomic resolution based on quantum tunnelling. In quantum tunnelling quantum particles cross a certain energy barrier that is higher than the particle's own energy. This section provides a qualitative description of how STM imaging works.

A vital part of an STM is its atomically sharp tip which is brought very close to a conducting surface. At a typical distance of about 0.3–1 nm [19] electron tunnelling through the vacuum barrier occurs upon applying a bias voltage ($V$) between tip and sample. The tunnelling current $I_t$ that arises is dependent on $V$ and exponentially on the tip-sample distance. Therefore, measuring $I_t$ provides information about the tip-sample distance.

The tip is connected to piezoelectric scanning tubes (piezos) mounted in x, y and z direction. Piezos alter in length when different voltages are applied on them. While $I_t$ is measured, the piezos laterally move the tip to scan the sample surface [19]. During scanning, differences in tip-surface distance will change the tunnelling current. A feedback loop makes sure that the tip height is constantly altered to maintain a constant $I_t$. While scanning, the height of the tip is recorded and plotted as a function of lateral position resulting in a topographic image of the sample surface.

Alternatively, scanning over the surface at constant height ($z$) and record and plot $I_t$ as a function of lateral position, also results in an image of the sample surface. Because no feedback loop is needed, constant $z$ mode is faster than constant $I_t$ mode. However, in constant $z$ mode one risks to damage the tip when at a particular place on the sample the surface is higher than the preset tip height. Therefore, constant $z$ mode can only be used on a flat surface. In addition, $I_t$ decreases exponentially with tip-surface distance. Hence, there will be no linear scaling in the $I_t$ image.

A final note on the STM regards the tip-surface distance. Increasing $I_t$ for constant $V$ will be achieved by decreasing the tip height allowing for more tunnelling. In contrast, increasing $|V|$ while keeping constant $I_t$ will be achieved by decreasing the tip height. Another factor that indirectly influences the tip-surface distance, is the amount of electronic states involved in tunnelling. These are all states at the tip location with energies between the Fermi level and $V$. Moreover, at specific energies an arbitrary amount of electronic states exists. So in practice, the tip-sample distance is dictated by the $I_t$ and $V$ settings.

## 2.2   Scanning Tunnelling Spectroscopy

Apart from producing topographic images of a sample surface, an STM set-up can also be used for so-called Scanning Tunnelling Spectroscopy (STS). In STS the differential conductance ($dI/dV$) as a function of $V$ is measured at a certain position. $dI/dV$ is proportional to the LDOS [20]. The LDOS represents the proportion of states that are to be occupied by electrons at each energy, at a certain position on the sample.

The electronic states of the tip, which usually are not of interest, are also affecting $dI/dV$ measurements [7]. To account for this fact, background STS spectra can be taken at positions unaffected by (deliberate) surface state deficiencies. Consequently, the $dI/dV$ spectra of interest can be divided by the background spectra or, alternatively, the background can be subtracted from the spectra of interest. By doing so, artefacts from the tip states (affecting all spectra) are minimised in the spectra of interest.

Apart from taking $dI/dV$ spectra, STS can also be used to obtain $dI/dV$ maps. In the latter case the tip position is varied at constant $V$ instead of conversely. Such maps enable imaging of the Density Of States (DOS) for a larger portion of the surface at an energy of interest.

## 2.3   Atom manipulation

A third functionality of the STM is its ability to manipulate adatoms on the surface of the sample. Manipulation of adatoms can be divided into vertical and lateral manipulations [13]. The latter will be most important in this thesis and is discussed in more detail here.
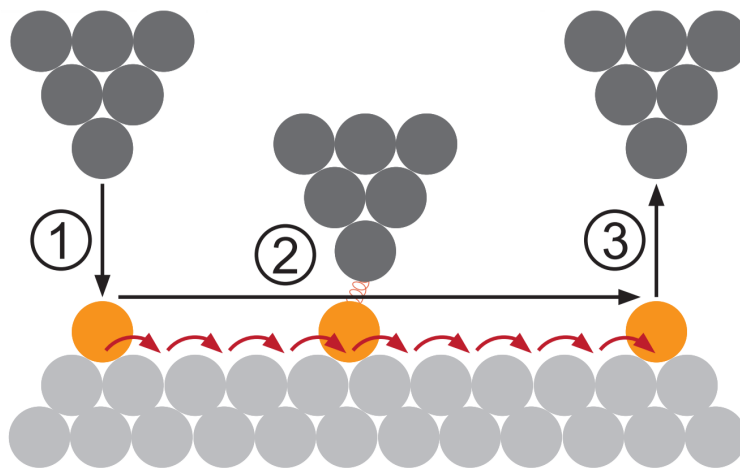


**Figure 1:** Schematic drawing of lateral manipulation of adatoms in the pulling mode. The STM tip (dark grey) is brought close to an adatom (orange) reaching an attractive force between the two (step 1). The tip is then moved laterally pulling the adatom with it over the sample surface (light grey) (step 2). When the tip is at the desired position, it is retracted again leaving the adatom at a new location on the sample surface (step 3). Figure taken from Ref. [21].

A schematic example of lateral manipulation in the pulling mode is shown in Figure 1. The first step of lateral manipulation is bringing the tip closer to an adatom so that attractive Van der Waals forces occur [22]. When consequently the tip is moved laterally over the surface, the adatom can be either pulled, slided or pushed with it over the surface [13]. Which of these three processes occurs, depends on the tip position with respect to the adatom. Finally, the tip is pulled back and the adatom is left at a new position.

Apart from moving adatoms, the tip can also be used to pick up atoms. When the tip is brought near an *ad*atom, it can attach to the tip. Retracting the tip will then pick up the adatom. In the case of Ag, it will help to not position the tip next to, but right above the adatom to prevent the adatom to move laterally. When the tip is brought near an atom that is in the substrate, there is a chance that attractive forces pull the atom onto the surface making it an *ad*atom [18]. Similarly, there is also a chance that the same attractive forces pull an atom from the *tip* onto the surface.

When an adatom is picked up to consequently put an atom form the tip on the surface at a different location, as described above, it could both be the same atom. This is effectively a technique to move adatoms. In contrast to lateral manipulation (Figure 1), this is called vertical manipulation.

## 2.4   Quantum corrals

In a crystalline metal, there is a periodic potential which is abruptly terminated at the surface. This abrupt change in the potential gives rise to electronic states that are uniquely localised a few Å from the surface, called Shockley or Tamm surface states [25, 26]. When a surface state is able to (nearly) freely propagate along the surface, it can be approximated as a Two-Dimensional Electron Gas (2DEG).
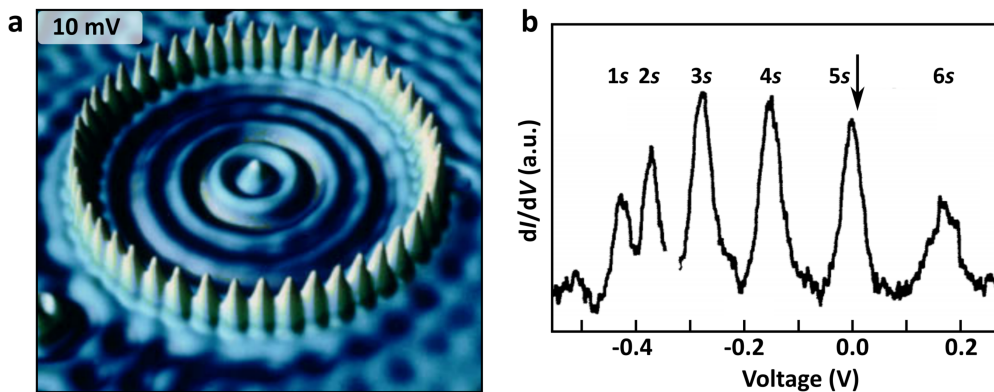


**Figure 2: (a)** A $dI/dV$ map taken at 10 mV of a circular ring of 48 Fe atoms placed on a Cu(111) surface by Crommie *et al.* A standing wave pattern is observed inside the quantum corral. **(b)** Background corrected $dI/dV$ spectrum taken at the centre of the corral depicted in (a). Distinct peaks are observed which are labelled 1$s$-6$s$ following the "particle-in-a-round-box" model. The arrow indicates the voltage at which the $dI/dV$ map depicted in (a) is taken. Reproduced from Refs. [5, 23, 24].

By manipulating adatoms as described in the previous section, adatoms can be arranged in a circular ring on the surface creating a so-called quantum corral. This was first done by positioning 48 Fe atoms on a Cu(111) surface [23], see Figure 2a. The adatoms, which impose a potential barrier, confine the enclosed 2DEG. A $dI/dV$ spectrum taken at the centre of the corral shows peaks at discrete energy levels indicating quantisation of the system, see Figure 2b.

The quantised states inside a quantum corral can be understood in terms of a particle-in-a-(round-)box model [23, 28]. This model provides the description of a quantum particle confined inside an infinitely deep potential well. Following the particle-in-a-(round-)box model, the wave functions will be characterised by their principle and angular quantum numbers, $n$ and $l$, respectively [8]. The ground state ($n = 1$, $l = 0$) will have no nodes in the wave function with a maximum LDOS in the centre of the corral, see Figure 3a. The next state in energy ($n = 1$, $l = 1$), will have one node in the centre of the corral with a ring of higher LDOS around it, see Figure 3b. In analogy to atomic orbitals of hydrogen, these states are called the $1s$-like and $1p$-like states, respectively. This analogy can be extended to higher energy states although it becomes less accurate. However, the $1s$-like and $1p$-like states will be most important in this thesis. Figure 3 visualises the analogy between these states and $1s$ and $2p$ orbitals in the hydrogen atom. In Figure 3a no node and in Figure 3c no nodal plane is present in the centre ($s$-like). Whereas a node and a nodal plane are
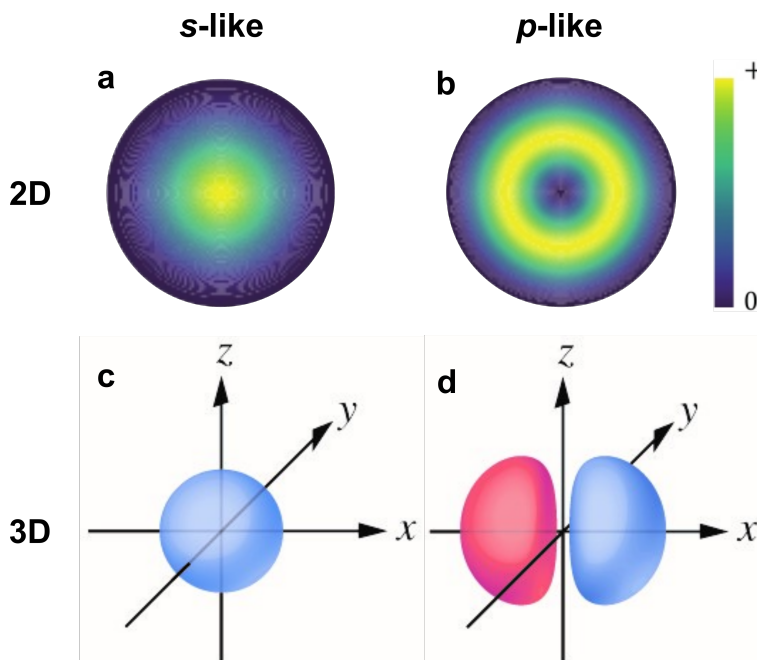


**Figure 3: (a, b)** $|\Psi|^2$ for a circular quantum corral as calculated with the particle-in-a-round-box model. (a) shows the $1s$-like state and (b) the $1p$-like state. **(c, d)** Three-dimensional visualisation of the $1s$ (c) and $2p$ (d) orbitals of the hydrogen atom. These four images visualise the analogy between the electronic states of in-plane artificial atoms (a, b) and that of the hydrogen atom (c, d). Images taken from Refs. [8, 27].

present in Figures 3b and d, respectively ($p$-like). Following this analogy, quantum corrals are sometimes indicated as (in-plane) artificial atoms.

### 2.4.1   Coupling two corrals: dimer

Just like two hydrogen atoms can bond and form a hydrogen molecule, two artificial atoms can also bond and form a dimer. Such a dimer can be realised by building two corrals adjacent to one another and leaving out the barrier between them. In analogy to molecular orbitals in a hydrogen molecule, the electronic states in a dimer can be seen as a superposition of the states of the individual corrals. The $1s$-like states for instance, superimpose a bonding and an anti-bonding $1s$-like state in the dimer. And similar for the $1p$-like states.

### 2.4.2   Peak broadening

In an ideal particle-in-a-box model, electronic states correspond to discrete energies. As can be seen in the $dI/dV$ spectrum in Figure 2b however, peaks corresponding to electronic states do not correspond to one discrete energy. Instead, the peaks exhibit a certain width. The peak broadening causes certain limitations in experiments. For instance, too much broadening makes it difficult to distinguish between certain states which are close in energy.

Peak broadening is partially a result of coupling of the 2DEG surface state with the bulk states [5]. This coupling is caused by scattering of the surface state electrons into bulk states. Scattering occurs in electron-electron or electron-phonon interactions, or when a surface state electron is scattered by an adsorbate or step edge. Scattering at a CO adsorbate is mainly the cause for peak broadening in $dI/dV$ spectra on the CO/Cu(111) system [5].

Another cause for peak broadening, is the coupling of the confined states, through the corral boundary, with the surrounding 2DEG [29]. The extent to which the confined states overcome the boundary are determined by the energy of these states and the firmness of the boundary. For higher energies coupling with surrounding 2DEG increases and for firmer boundaries it decreases. The firmness of the boundary can be increased by creating a denser adatom boundary and/or by using adatoms which induce a higher potential barrier.

When the size of a corral is decreased, the confinement increases. Thereby, the amount of scattering as well as the energies of the quantum states increase. Therefore, peak broadening will increase with decreasing corral size due to both of the mentioned broadening effects.

### 2.4.3   Muffin-tin

A theoretical model to describe artificial atoms and lattices, is the muffin-tin model. The muffin-tin model can be used to calculate the LDOS and thus predict experimentally obtained $dI/dV$ values.

In the muffin-tin model, adsorbates of artificial atoms are interpreted as potential barriers for the 2DEG for which the complex particle-in-a-box is solved. The Schrödinger equation is solved to obtain the wave functions corresponding to energies from the lowest up to an

indicated maximum energy value. From these wave functions the LDOS can be extracted.

To calculate the LDOS of an electronic lattice and simulate $dI/dV$ spectra taken on it, several parameters need to be provided as input. These parameters are the radius of the potential barrier and their potential height, the effective electron mass, the maximum number of wave functions to be included in the calculation, the size of the simulation box, and a Lorentzian broadening. The latter needs to be provided to simulate peak broadening in $dI/dV$ spectra. Unknown input parameters can be adjusted to make the muffin-tin output concur with experimental $dI/dV$ spectra. Consequently, unknown input parameters can be determined by fitting to experimental measurements. In particular, this is done to determine the potential height of adatoms.

The interested reader can find a more in-depth explanation of the muffin-tin model and how to perform such calculations in for example Ref. [30].

## 2.5   Thin Ag film on a Si(111) wafer

In this thesis, a Si(111) wafer covered with Ag monolayers is used to built quantum corrals. In this section, the surface reconstruction as well as the surface state of this particular surface is discussed.

Clean Si(111) undergoes a surface reconstruction to a thermodynamically stable $7 \times 7$ structure at temperatures above 300 °C [31]. Disposing one single monolayer of Ag atoms onto the Si(111)$7 \times 7$ surface, makes a Si(111)-$\sqrt{3} \times \sqrt{3}$-Ag surface the most stable reconstruction [32]. This surface has several surface states of which the one lowest in energy can be approximated as a 2DEG [33]. When the number of Ag monolayers is increased, the surface reconstruction gradually changes into that of Ag(111). At what number of monolayers exactly the reconstruction changes from a Si(111)-$\sqrt{3} \times \sqrt{3}$-Ag into a Ag(111)/Si(111) surface, is unknown. However, at seven monolayers a Ag(111)/Si(111) surface has been observed [16]. The 2DEG surface state offset, i.e. the energy relative to the Fermi level at which the 2DEG starts to exist, decreases with the number of Ag monolayers. At seven monolayers the 2DEG surface state offset is at +26 meV and decreases to −51 meV at 40 monolayers [16]. Further increasing the number of Ag(111) monolayers will eventually bring the surface state offset at that of bulk Ag(111), i.e. −63 meV [34]. Regardless of the number of Ag layers, the 2DEG surface state offset will remain inside the Si band gap which ranges from −585 to +585 meV [15].

When Ag is deposited on a Si(111)$7 \times 7$ surface at room temperature, a Ag layer with a high island density, i.e. not flat, is formed [35]. Upon heating to temperatures above 200°C, Ag islands on the surface become unstable and anneal into larger islands, i.e. flatten out [35]. A flat surface gives rise to an undisturbed surface state which is then allowed to behave as a 2DEG. A flat surface and an undisturbed 2DEG surface state are requisites in order to realise quantum corrals using an STM.

Scanning the Ag(111)/Si(111) surface inside the Si band gap with an STM has a noteworthy implication. Since in the band gap the bulk Si(111) does not conduct any electrical

current, all the tunnelling current has to go through the Ag layer. Because the Ag layer is very thin and might not be homogeneously covering the Si(111) wafer, its conductivity can be relatively low. Especially for Ag layers thinner than 2.2 monolayers [36]. Therefore, to reach a certain tunnelling current the STM tip generally has to come closer to the surface than e.g. on Cu(111) which has high conductivity.

# 3   Methods

## 3.1   STM setup

A commercial Scienta Omicron low temperature STM was used to carry out the experiments. The setup consists of a measuring chamber and a preparation chamber. In both chambers ultrahigh vacuum ($p = 10^{-11}$ - $10^{-9}$ mbar) is maintained by an ion getter pump and, occasionally, a titanium sublimation pump or a turbo pump. The measuring chamber operates at a temperature of around 4.5 K accomplished by a liquid helium filled cryostat inside a liquid nitrogen filled cryostat.

## 3.2   Scanning Tunnelling Spectroscopy

STS was performed in controlled height mode while modulating the bias voltage with an amplitude (root mean square) of 3 or 10 mV at a frequency of 769 Hz, using a lock-in amplifier.

All STS spectra of a single measurement series were acquired with the same tip. Each spectrum was recorded double: one from starting bias voltage to ending bias voltage, forward, and one and backwards. Background spectra were taken and averaged. For measurements on Corral 1 (see section 4.2), background spectra were taken outside the corral at a single position. For measurements on the other lattices, background spectra were taken on consecutive positions in a straight line. Inside the lattices spectra were done five or seven times at the same position and averaged. The bias voltage range at which spectra were taken in Corral 1, the Dimer, and Corral 2, were from $-0.7$ to 0.6 V, $-0.2$ to 0.4 V or $-0.1$ to 0.5 V, respectively (see sections 4.2 to 4.4). The resolution in $V$ is 2 mV.

In order to maximise the signal-to-noise ratio for all bias voltages, a so-called varied-$z$ technique was used. In this technique, the tip height is decreased with bias voltage values closer to 0 V. Before the tip height can be altered, the constant $I_t$ feedback loop is turned off.

## 3.3   Sample and tip preparation

*Two* samples were prepared. The preparation was carried out in the preparation chamber and started with cleaning Si wafers. In 5 minutes they were heated to 900 °C by running a direct current trough the wafers, and left there for one hour. One of the two wafers had not been cleaned since it last came into the vacuum, and was left for five hours. Then the wafers were flashed to about 1200 °C for a maximum of 30 seconds. Flashing was repeated as many times as needed until the pressure would not exceed a raise of $0.7 \cdot 10^{-9}$ mbar. After cleaning, the wafers were put in the STM to confirm that they were properly clean and showed a clear Si(111)7 × 7 pattern.

Consequently, an evaporator, set at 1 kV and directed at the wafers, bombarded Ag-ions onto the wafers with a flux of 15 nA at room temperature. For *sample 1*, the evaporation was ended after 20 minutes and for *sample 2* after 5 minutes. To establish atomically flat Ag terraces, the samples were annealed at about 550 °C after which they were left to cool

down slowly. Sample 1 was annealed for 20 minutes, sample 2 for 30 minutes.

An obliquely cut Pt/Ir tip covered with Cu at its apex was used. The tip was prepared on each sample by voltage pulses and gentle contact with the sample surface, making sure the tip would not get in contact with underlying Si. Once the tip provided sharp and symmetric imaging, adequate $dI/dV$ spectra, and reliable manipulation, it was considered satisfactory.

## 3.4   Atom manipulation

The scanning settings used while performing atom manipulations, were a tunnelling current of $I_t = 0.1$ nA and a bias voltage ranging between $V = -0.7$ to $-0.1$ V. On a flat part of the sample surface with as few scatterers as possible in the vicinity, quantum corrals were constructed. Atoms were placed on the surface roughly at the spot where they needed to be to construct the corral. The shape of the corral was then adjusted by lateral manipulation of the adatoms.

## 3.5   Data processing

The results presented in this thesis consist of constant current images, differential conductance spectra and fit parameters of peaks in them.

Using the software Gwyddion [37], the constant current images were processed. The images were flattened by plane subtraction. By means of two-dimensional Fast Fourier Transformation filtering, noise is filtered out of the images to obtain smoother images.

The differential conductance spectra were processed using Python programming [38]. Spectra taken at the same location were averaged, both their forwards and backwards. Corresponding background spectra taken at different locations were also averaged. Corresponding spectra which did not overlap properly, although rarely the case, were disposed. Background correction of spectra was performed by dividing spectra by the corresponding background. Muffin-tin calculations were performed on idealised versions of the lattices using a dedicated python package [39]. Values of muffin-tin input parameters were: radius of the potential barrier $r = 0.53$ nm, effective electron mass $m_{\mathrm{eff}} = 0.39 m_{\mathrm{e}}$, number of wavefunctions included $n = 300$, and a simulation box size scaling factor $b = 30$.

Peaks in background corrected spectra were fitted by Gaussian functions to obtain their energy and Full Width at Half Maximum (FWHM) values. An example of a 'good' Gaussian fit can be seen in the appendix, Figure 9. Peaks adjacent to other peaks, were fitted based only on their side not adjacent to another peak, see appendix, Figure 10. Peak energy and FWHM values obtained in different spectra representing the same electronic state, were averaged to obtain values for each separate state.

# 4   Results & Discussion

## 4.1   Atom manipulation

After sufficient tip preparation, manipulating atoms on the surface became possible. It was found that atoms either from the tip or the substrate could be placed on the sample by applying $\Delta z = -0.6$ to $-0.8$ nm. When this stopped working, $\Delta z$ was gradually increased to about $-1.0$ nm which mostly resulted in a much larger atomic cluster on the surface. This cluster could then partially be picked up by applying $\Delta z \approx -0.75$ nm. Placing atoms on the surface by $\Delta z = -0.6$ to $-0.8$ nm then became possible again and the cycle could be repeated.

Adatoms could be laterally moved by applying a single $\Delta z = -0.55$ to $-0.7$ nm *at the side* of the adatom, which would then move towards that side. The fact that the adatom moves towards the tip, suggests an attractive force between the sides of the adatom and tip apex. For manipulating longer distances the tip was kept down after applying $\Delta z$ and then moved laterally over the surface. This lateral movement was performed in constant $z$ without feedback loop. It was found that the adatoms were dragged with the moving tip over the surface. Such lateral manipulations of adatoms were not always successful. During part of the experiment statistics on these lateral manipulations were tracked. The scanning settings used while tracking lateral manipulations were $I_t = 0.1$ nA and $V = -0.7$ V. For applying a single $\Delta z$, all 15 tracked manipulations were successful at $\Delta z = -0.6$, $-0.65$ and $-0.7$ nm (11, 3 and 1 attempts, respectively). At $\Delta z = -0.55$ nm, 50% out of 28 attempts were successful. Most successful manipulations by dragging turned out to be at $\Delta z = -0.65$ nm with a success rate of 81% out of 31 attempts.

## 4.2   Corral 1

Corral 1 was realised on sample 1 by putting 12 atomic clusters in a circle with diameter of about 6.4 nm on the flat surface, see Figure 4a. The atomic clusters had a diameter ranging from 1.2 to 1.5 nm and originated from either the surface or the tip. Because the tip was prepared on the sample, its apex was probably covered with Ag. Therefore, the atomic clusters seen in Figure 4a presumably consist of Ag atoms. However, because the tip was initially covered in Cu, the atomic clusters could also consist of Cu atoms.

### 4.2.1   Experimentally obtained spectra

Several $dI/dV$ spectra were taken inside corral 1 at different locations. Figure 4b shows the spectra taken in the centre and about 1.2 nm right from the centre (see dots in Figure 4a) as well as corresponding muffin-tin predictions.

First of all, several peaks can be observed in the spectra depicted in Figure 4b. The spectra taken in the centre of the corral (blue solid line) show a relatively sharp and high peak at $-0.012$ V with a FWHM of 0.028 V and a broader peak around 0.211 V, FWHM $= 0.084$ V. Furthermore, an increased intensity centred around 0.35 V can be seen, but can not be distinguished as a clear peak.
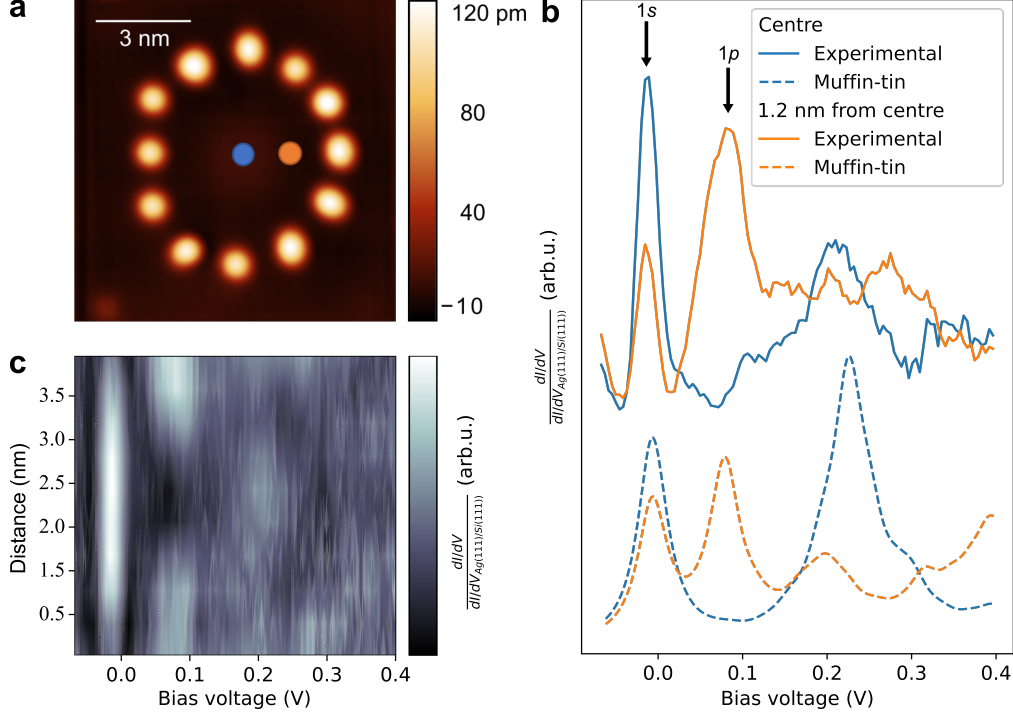
**Figure 4:** **(a)** A $10 \times 10$ nm$^2$ constant-current STM image of corral 1. The 12 adsorbates are atomic clusters presumably of Ag. The blue and orange dots give an indication of where spectra shown in (b) were taken. Imaging parameters: $I_t = 0.1$ nA, $V = -0.7$ V. **(b)** Background divided $dI/dV$ spectra acquired above corral 1 at the centre (blue solid line) and 1.2 nm right from the centre (orange solid line) and LDOS at these sites calculated using the muffin-tin model (dashed lines). The arrows indicate the bias voltages at which the $1s$-like and $1p$-like states were observed. **(c)** Contour plot of 11 spectra taken inside corral 1 horizontally from side to side through the centre.

Secondly, the spectra taken about 1.2 nm right from the centre (orange solid line) show a peak at $-0.014$ V, FWHM $= 0.026$ V. It is less intense than the blue peak at about the same energy. Moreover, an intense, slightly broader peak at 0.081 V, FWHM $= 0.066$ V is observed. For higher energies there is some discrepancy in intensity, but no distinct peak can be observed.

Taking into account the location where these peaks are observed leads us to clues. The $1s$-like state in a quantum corral has the highest intensity in the centre and decreasing intensity towards the edges, as is described in section 2.4. This seems to be what is observed in Figure 4b around $-0.013$ V. Therefore, it is plausible that a $1s$-like state has been observed around $-0.013$ V. Furthermore, the peak at 0.081 V observed 1.2 nm outside the centre is not observed in the centre for that same energy. This suggests a state with a node in the centre and could be attributed to the $1p$-like state. Finally, the second peak in energy observed in the centre at 0.211 V, could be attributed to the $2s$-like state.

Figure 4c shows a contour plot of 11 consecutive spectra taken horizontally through the centre. Looking at the same energies in Figure 4c as the peaks seen in Figure 4b, the prior suggestions are substantiated. The intensities around $-0.013$ V clearly show an $1s$-like state

with highest intensity in the centre and decreasing towards the edges. Around 0.08 V, a $1p$-like pattern is indeed observed with a node in intensity in the centre and higher intensities on either sides. Finally, around 0.21 V high intensity in the centre, two nodes on either side after which higher intensity again, are observed. Although the data are not as clear around 0.21 V, this could indeed be attributed to a $2s$-like state.

### 4.2.2   Muffin-tin results

The dashed lines in Figure 4b show LDOS spectra as calculated with the muffin-tin model. To account for peak broadening in the experimental $dI/dV$ spectra, a Lorentzian broadening of 20 mV is included. The muffin-tin spectra were fitted to the experimental spectra depicted in solid lines in Figure 4b. From the fitting, the potential of the potential barriers were determined to be 0.65 eV.

The blue dashed line in Figure 4b represents the muffin-tin calculated LDOS in the centre of the (idealised) corral. The peaks in the experimental spectrum (solid blue line) at $V = -0.012$ and 0.211 V are also shown in the muffin-tin. The orange dashed line represents the muffin-tin calculated LDOS 1.2 nm next to the centre. Here, the peaks in the experimental spectrum (solid orange line) at $V = -0.014$ and 0.0811 V are also visible at around the same energies. As in the experimental spectra the $1p$-like peak is higher than the $1s$-like peak. Around 0.2 V, the orange dashed line has a peak which is hardly visible in the experimental spectrum. Given that this peak is close in energy to the $2s$-like peak in the blue lines, it might also be attributed to this state. All in all the muffin-tin calculations seem to be well in agreement with the experimental observations.

## 4.3   Dimer

Corral 1 was expanded into a dimer by building an identical corral next to it and removing the adatom in between the two, see Figure 5a. The distance between the centres of the two adatoms at the opening was 3.1 nm. Spectra were taken at several locations in the dimer. Since corral 1 is duplicated to produce the dimer, it can be assumed that observed states in the dimer correspond to the states in corral 1 (see section 4.2) for similar energies.

### 4.3.1   $1s$-like and $1p$-like bonding and anti-bonding states

Spectra taken at the centre, the centre of the right corral, and the left edge of the dimer (see dots in Figure 5a) are shown in solid lines in Figure 5b. Corresponding muffin-tin calculations are shown in dashed lines in Figure 5b.

For corral 1 a $1s$-like state exists around $V = -0.01$ V, as is argued in section 4.2. Around $V = -0.01$ V, three peaks can be observed in Figure 5b. An intense peak at $-0.021$ V, FWHM 0.056 V (solid orange line), and two less intense peaks at $-0.033$ V, FWHM 0.036 V (solid blue line) and $-0.019$ V, FWHM 0.040 V (solid green line). Since this is a dimer of two connected corrals of equal size to corral 1, one can expect that the $1s$-like states of each corral interfere to form a $1s$-like bonding and a $1s$-like anti-bonding state (section 2.4.1). In
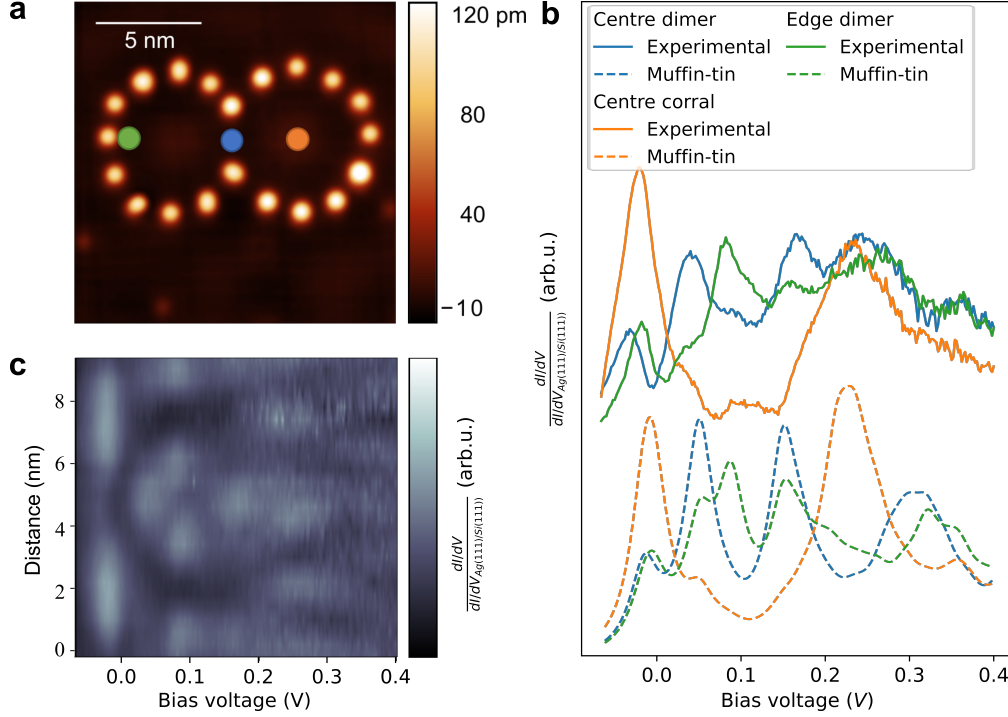
**Figure 5:** **(a)** A $15 \times 15$ nm$^2$ constant-current STM image of the dimer. The 20 adsorbates are atomic clusters presumably of Ag. The green, blue, and orange dots give an indication of where spectra shown in (b) were taken. Imaging parameters: $I_t = 0.1$ nA, $V = -0.2$ V. **(b)** Background divided $dI/dV$ spectra acquired above the dimer at the left edge (green solid line), centre (blue solid line) and centre of the right corral (orange solid line). The dashed lines depict the LDOS at these three sites calculated using the muffin-tin model. **(c)** Contour plot of 26 spectra taken inside the dimer horizontally from side to side through the centre.

the centre of the dimer the $1s$-like bonding should exhibit its highest intensity at a lower energy than the anti-bonding state. The peak at $-0.033$ V observed in the dimer centre, is thus expected to represent the $1s$-like bonding state. The peak at $-0.019$ V observed at the left edge, must then represent the $1s$-like anti-bonding state, which is higher in energy. At the centre of either corrals, both $1s$-like states should be observable. Therefore, the peak at $-0.021$ V must be a superposition of both states. Attributing the peak at $-0.021$ V to a superposition of two states explains its higher intensity and broader shape.

A similar reasoning can be used to appoint the $1p$-like bonding and anti-bonding states. In section 4.2, it is argued that the $1p$-like state exists around $V = 0.08$ V. In the centre of both corrals the $1p$-like state should not be observable, which is the case around 0.08 V. In the centre of the dimer, the $1p$-like bonding state should and the anti-bonding state should not be observable. In contrast, at the edge of the dimer, the LDOS of the $1p$-like anti-bonding should be higher than for the bonding state. This is what the peaks at 0.042 V (centre dimer, blue solid line) and 0.085 V (left edge, green solid line) exhibit. The peaks at 0.042 V and 0.085 V, can thus be attributed to the $1p$-like bonding and anti-bonding states, respectively.

The muffin-tin calculated LDOS in Figure 5b simulates the experimentally obtained quite

well. Each of the peaks discussed above is observed in the muffin-tin.

A contour plot of 26 consecutive spectra taken horizontally through the dimer is shown in Figure 5c. The contour plot depicted in Figure 5c substantiates the prior claims. Firstly, around $-0.1V$ $1s$-like states are observed in both corrals. Near the edges of the dimer (upper and lower sides in the plot) the intensity leans towards higher energy (anti-bonding). In addition, near the dimer centre (around 5 nm in the plot) the intensity leans towards lower energy (bonding). Secondly, around 0.85 V $1p$-like patterns are clearly visible in both corrals with in between the two lower intensity (anti-bonding). Around 0.4 V, high intensity is observed in the dimer centre with two nodes in each corral centre (bonding).

The $2s$-like peak observed in corral 1 also seems to be observed in the centre of the right corral. However, no clear signs of corresponding bonding or anti-bonding states are found. All peaks observed for bias voltages above 0.1 V are left out of this discussion since they exhibit much overlap and are difficult fit.

### 4.3.2   Increased dimer coupling

The dimer was altered by moving the two atom barriers at the corners between the two corrals to leave a 1 nm broader opening by, see Figure 6a. LDOS measurements and calculations were repeated on the altered dimer and are shown in Figures 6b and c. These LDOS data differ from the LDOS data in the original dimer (Figures 5b and c). However, the same states are observed.

State energies were determined to check the difference between corresponding bonding and anti-bonding states with respect to that of the original dimer. Due to the increased opening between the two corrals, the spatial overlap of their wave functions should be increased too. Therefore, one would expect the bonding states to lower and the anti-bonding states to rise in energy.

For the $1p$-like states, the energy difference indeed increased by 7 meV form 0.043 eV to 0.050 eV. For the $1s$-like states on the other hand, the energy difference decreased by 1 meV from 0.015 eV to 0.014 eV, see table 1. The latter is against the expectations. However, 1 mV is less than the bias voltage resolution of 2 mV. Therefore, a difference of 1 meV is smaller than the error margin of the determination and thus not significant. So it might still be the case that the bonding for the $1s$-like states increased by an amount too small to be observed. Such a small increase is plausible since we have seen that the coupling of the $1s$-like states of each corral is considerably smaller (about a factor three) than for the $1p$-like states. Thus,

**Table 1:** Energy difference between $1s$-like and $1p$-like bonding and anti-bonding states in the original dimer and the dimer with increased coupling.

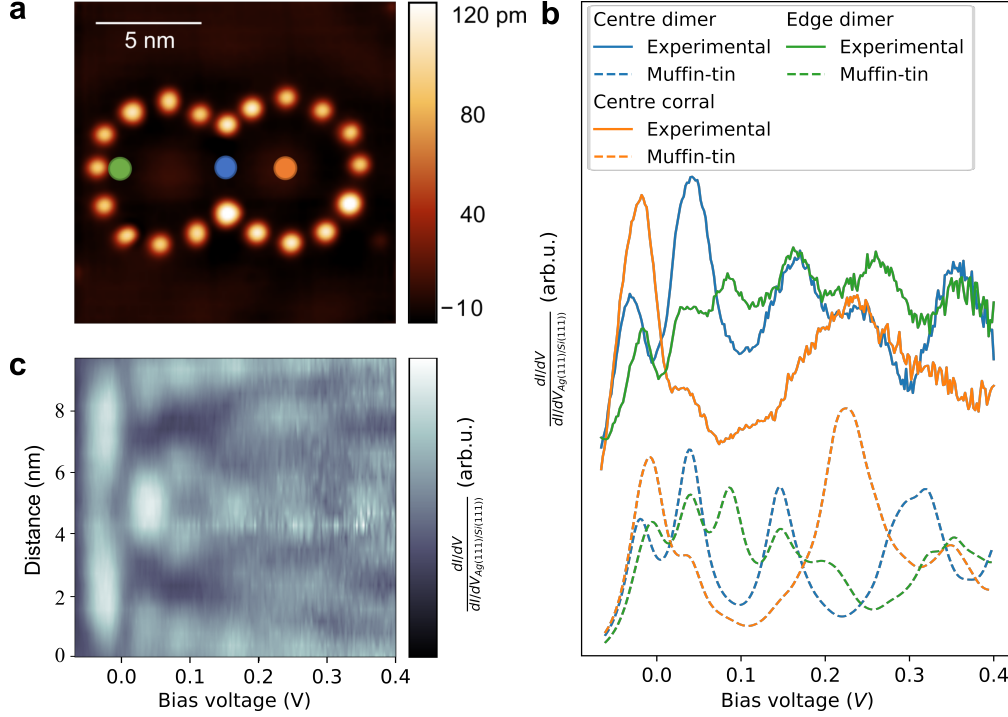| State type | Original | Increased coupling |
|---|---|---|
| $1s$-like | 0.015 eV | 0.014 eV |
| $1p$-like | 0.043 eV | 0.050 eV |

**Figure 6:** **(a)** A $15 \times 15$ nm$^2$ constant-current STM image of the adjusted dimer. The 20 adsorbates are atomic clusters presumably of Ag. The green, blue, and orange dots give an indication of where spectra shown in (b) were taken. Imaging parameters: $I_t = 0.1$ nA, $V = -0.2$ V. **(b)** Background divided $dI/dV$ spectra acquired above the adjusted dimer at the left edge (green solid line), centre (blue solid line) and centre of the right corral (orange solid line). The dashed lines depict the LDOS at these three sites calculated using the muffin-tin model. **(c)** Contour plot of 26 spectra taken inside the adjusted dimer horizontally from side to side through the centre.

one expects the energy difference between the $1s$-like states to change considerably less than the $1p$-like states, which was 7 meV.

## 4.4   Corral 2

On sample 2, corral 2 was realised with a diameter of 4.8 nm, see Figure 7a. Several $dI/dV$ spectra were taken at different locations inside the corral.

Figure 7b shows spectra taken at the centre and right from the centre. Most peaks observed in the spectra taken above corral 2 are asymmetric. An unambiguous reason for this asymmetry could not be found. The asymmetry was observed in the non background corrected spectra. Hence, the background correction did not have an influence.

Due to their asymmetric shape, it was not possible to properly fit full peaks. Instead, only half the peaks were fitted. By doing so, the position of the peaks could be determined. However, the FWHM values which resulted from these fits, differ considerably. This is because the left sides of the peaks are much steeper, resulting in an underestimation of the FWHM and vice versa for the right sides. Nonetheless, on the basis of these over- and underestima-
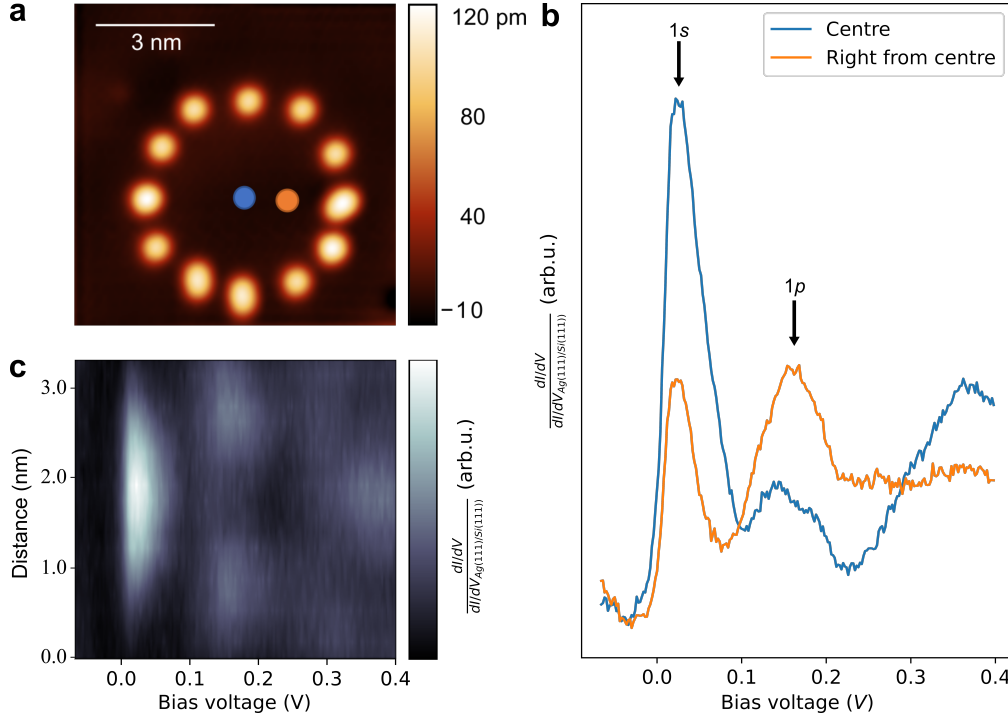
**Figure 7:** **(a)** A $8 \times 8$ nm$^2$ constant-current STM image of corral 2. The 12 adsorbates are atomic clusters presumably of Ag. The blue and orange dots give an indication of where spectra shown in (b) were taken. Imaging parameters: $I_t = 0.1$ nA, $V = -0.1$ V. **(b)** Background divided $dI/dV$ spectra acquired above corral 2 at the centre (blue) and right from the centre (orange). The arrows indicate the bias voltages at which the 1$s$-like and 1$p$-like states were observed. **(c)** Contour plot of 21 spectra taken inside corral 2 horizontally from side to side through the centre.

tions as well as *ad hoc* measurements of the peak widths, FWHM values were estimated.

Figure 7c shows a contour plot of 21 consecutive spectra taken horizontally from side to side through the centre of corral 2. From Figures 7b and c, the 1$s$-like and 1$p$-like states can be deduced. In between 0 and 0.1 V high intensity at the centre, blue solid line (0.023 V, FWHM $= 0.050 \pm 0.005$ V), and low intensity right from the centre, orange solid line (0.024 V, FWHM $= 0.045 \pm 0.01$ V), are observed. These peaks can be attributed to the 1$s$-like state. The 1$p$-like state is observed between 0.1 and 0.2 V with higher intensity right from the centre (0.161 V, FWHM $= 0.084 \pm 0.02$ V) than at the centre (0.143 V). Finally, at 0.38 V highest intensity at the centre and nodes on either sides seems to be observed in Figure 7c. The blue solid line in Figure 7b confirms a higher intensity at the centre at 0.38 V. A 2$s$-like state can therefore be attributed at around 0.38 V.

At the centre of corral 2, a peak is observed for the 1$p$-like state which is unexpected. A possible explanation could be that the "centre" spectra, were not taken exactly at the centre, rather slightly besides it. Another explanation, although less probable, could be the fact that corral 2 is not perfectly symmetric. This could result in the 1$p$-like state not having a single node in the centre.

The energies at which the 1s- and 1p-like states are observed in corral 2, are about 35 mV and 70 mV higher than for corral 1 and the dimer, respectively. This is caused by the fact that corral 2 is smaller and therefore confines the surface state electrons more. The fact that corral 2 is realised on a different sample could also have played a role in this, perhaps due to a shift in surface state offset. A decrease in Ag layer thickness, should cause the surface state offset to go up in energy [16]. It could not be determined whether a shift in surface state offset occurred between sample 1 and sample 2.

## 4.5   Comparing peak broadening

Peaks in different spectra representing the same state in the same lattice, should in principle exhibit the same broadening. Accordingly, FWHM and bias voltage values of all peaks representing 1s-like or 1p-like states in the same lattice, were averaged. In case of the dimers this was done for the 1s-like and 1p-like bonding and anti-bonding states. The results are summarised in Figure 8.

Apart from the spectra mentioned in previous sections, five more spectra are included in the data presented in Figure 8. These five spectra were taken at about 1.2 and 2.4 nm below the centre in corral 1, the top right quarter of corral 2, and the right edge and centre of the right corral of the adjusted dimer.

The FWHM values in Figure 8 seem to be going up with increasing state energy. This trend is to be expected since for higher state energies, the confined electrons inside a quantum corral more easily overcome the potential barrier. Therefore, for higher state energies the confined electrons couple more with the 2DEG surrounding the corral which causes peak broadening (see section 2.4.2).

### 4.5.1   Comparing sample 1 and sample 2

Comparing the FWHM values of corral 1 and the dimer with corral 2, might give clues on the differences induced due to the difference in thickness of the Ag layer. However, looking at Figure 8 the FWHM values of corral 2 (red dots) seem to be part of the trend observed on sample 1. In Figure 8, the FWHM values corresponding to the 1s-like and 1p-like states in corral 2, belong to higher energies. This is due to the fact that corral 2 was smaller than corral 1 and the dimers. Smaller corrals cause more electron confinement, thus higher state energies and more peak broadening. Moreover, the relatively large uncertainty in FWHM values for corral 2 (see section 4.4) and the fact that there was only one corral realised on sample 2, makes it difficult to see the trend on sample 2. Therefore, no distinction can be made between the two samples in terms of energy broadening they yield.

### 4.5.2   Comparing with CO/Cu(111)

Overall, the FWHM values yielded on the Ag(111)/Si(111) system lies between 25 and 80 mV, see Figure 8. This result seems favourable compared to the reported Lorentzian broad-
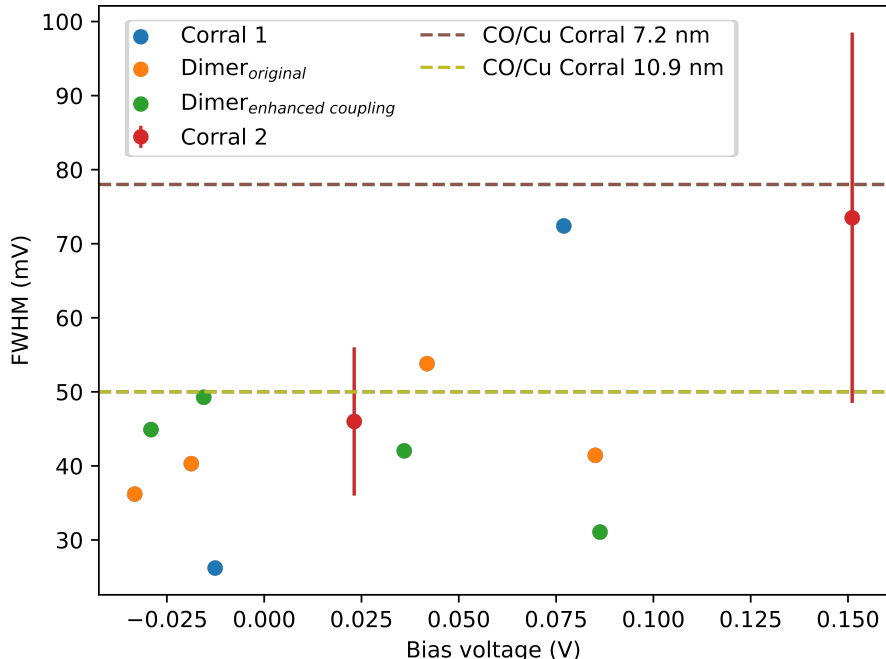
**Figure 8:** Averaged FWHM values of $1s$-like and $1p$-like states observed in corral 1 (blue dots), the dimer, both the original (orange dots) and the adjusted one (green dots), and corral 2 (red dots). The FWHM values are plotted against the bias voltages at which corresponding peaks were observed. The dashed lines indicate the median FWHM of corrals with diameter 7.2 nm (brown dashed line) and 10.9 nm (olive dashed line) built on the CO/Cu(111) system [30].

ening[3] of approximately 80 meV on a CO/Cu(111) system [5]. The FWHM values between 25 and 80 mV reported here (Figure 8) would classify as less broadening than "approximately 80 mV".

However, as was discussed in section 2.4.2, broadening in $dI/dV$ spectra taken at quantum corrals depends on the corral size. Therefore, when comparing FWHM values between different systems, corral size ought to be taken into account. Rian A.M. Ligthart and Thomas S. Gardenier [30] have reported Gaussian FWHM values of peaks observed in $dI/dV$ spectra taken at quantum corrals built on a CO/Cu(111) system. Here, two corrals with diameter 7.2 nm and 10.9 nm were observed. On the quantum corral with diameter 7.2 nm the FWHM median was approximately 78 mV with lower and upper limits of 30 and 120 mV, respectively. On the corral with diameter 10.9 nm, the FWHM median was approximately 50 mV with lower and upper limits of 15 and 120 mV, respectively. These FWHM medians are plotted as dashed lines in Figure 8.

It has to be noted that comparing FWHM values obtained from quantum corrals on different systems is not trivial. An important factor in the behaviour of electronic states in a quantum corral, is the effective electron mass. On different systems with different electron masses, corrals of identical size can not be directly compared. In the case of the CO/Cu(111)

---

[3]Lorentzian broadening is defined as the FWHM value of a Lorentzian curve, which, on its turn, is equivalent to the FWHM value of a Gaussian curve with the same height.

and Ag(111)/Si(111) systems the effective electron masses differ. On Cu(111) the effective electron mass at the surface is around $0.40m_e$ [5, 40]. On the Ag(111) surface, an electron mass of about $0.37m_e$ was reported [40]. For the Ag(111)/Si(111) system this might be similar. The difference in effective electron mass on each system is not immense. Therefore, FWHM values obtained on corrals in the Ag(111)/Si(111) and CO/Cu(111) systems can be compared with caution.

The corral with diameter 7.2 nm comes closest in size to corral 1 (6.4 nm) and corral 2 (4.8 nm). Still this corral is larger and therefore has an advantage with respect to broadening. Nevertheless, FWHM values in the 7.2 nm corral are in the order of several tens of millivolts larger than what was found in any of the lattices presented in this thesis, see Figure 8.

The corral with diameter 10.9 nm has, as expected, significantly lower FWHM values compared to that with diameter 7.2 nm. Since the diameter is even larger, its FWHM values can not be compared directly with the values obtained from the Ag(111)/Si(111) system in this thesis. However, it does substantiate the thought that a corral of, say, diameter 6.4 nm on a CO/Cu(111) system would exhibit higher FWHM values than the 7.2 nm corral, and thus even higher compared to corral 1 (6.4 nm).

All in all, the analyses in the previous paragraphs suggest that a quantum corral built on the Ag(111)/Si(111) system yields less broadening than a quantum corral of equal size on the CO/Cu(111) system. Moreover, the difference in broadening can be expressed in Gaussian FWHM values of the order of tens of millivolts. However, because the exact effective electron masses in each system are unknown, the conclusion cannot be made with absolute certainty.

### 4.5.3   Comparing with the expectations

On CO/Cu(111) the Lorentzian broadening of approximately 80 meV is mainly caused by coupling with bulk states [5]. So, when no bulk states would be present, peak broadening in $dI/dV$ spectra would drastically decrease. In theory, on a sufficiently thin Ag layer on Si(111), there will be no bulk states to couple with. Yet, the FWHM values observed on the Ag(111)/Si(111) system (Figure 8) were still in the order of tens of millivolts as on the CO/Cu(111) system. It can therefore be questioned whether bulk states were present in the Ag(111)/Si(111) samples.

The fact that at the surface a Ag(111) and not a $\sqrt{3} \times \sqrt{3}$-Ag reconstruction was observed, tells us that more than about five Ag monolayers on Si(111) were present (see section 2.5. How many monolayers there were exactly, is unknown. Therefore, it might be the case that sufficient Ag monolayers were present for bulk states to arise. To rule out the possibility that bulk states are present in a Ag(111)/Si(111) system (in the band gap of Si), a thinner Ag layer must be tested.

# 5   Conclusions

Two Si(111) wafers were covered by a Ag layer each with different thickness: sample 1 and sample 2. On the Ag(111)/Si(111) systems prepared, it was shown that atom manipulation is possible. Placing atoms from either substrate or tip on the surface, picking up adatoms, as well as laterally move adatoms, were proved to be possible.

By atom manipulation, two quantum corrals were realised. One with diameter 6.4 nm on sample 1 and one with diameter 4.8 nm on sample 2. The former was also extended into a dimer. In $dI/dV$ spectra taken inside the quantum corrals, $1s$-like, $1p$-like and $2s$-like states were observed. In the dimer it was observed that $1s$-like and $1p$-like states interfered into a bonding and an anti-bonding state. When the coupling area between the two corrals in the dimer was increased, an increase in electronic coupling was observed. Muffin-tin calculated LDOS spectra were well in accordance with experimental observations. From muffin-tin calculations, the potential of the potential barriers was determined to be 0.65 eV.

Peaks in $dI/dV$ spectra corresponding to $1s$-like and $1p$-like states were fitted by Gaussian functions to obtain their FWHM. From analysing FWHM values no distinction between sample 1 and sample 2 could be found in terms of FWHM values found. The FWHM values obtained were compared with Gaussian FWHM values for corrals on a CO/Cu(111) system with diameter 7.2 nm and 10.9 nm. The analysis suggested that quantum corrals exhibit less broadening on the Ag(111)/Si(111) system than on the CO/Cu(111) system. The difference in broadening was determined to be in the order of tens of millivolts, expressed in Gaussian FWHM values, for corrals of the compared sizes.

Lastly, it was questioned whether the Ag layers on sample 1 and sample 2 had bulk states. FWHM values found were higher than expected for a Ag(111)/Si(111) system without bulk states. Therefore, it might have been the case that the Ag layers on sample 1 and sample 2 were thick enough for bulk states to arise.

# 6  Outlook

Several options can be considered to further develop a system on which electronic structures can be simulated with an increased energy resolution.

First of all, to further improve the energy resolution in $dI/dV$ spectra on a Ag(111)/Si(111) system, thinner Ag layers must be deposited. A thinner Ag film reduces the probability of bulk state presence, and thus could increase the energy resolution. Making the Ag film too thin however, results in a $\sqrt{3} \times \sqrt{3}$-Ag surface reconstruction on which atom manipulation is not guaranteed to be possible.

Secondly, instead of Ag, a different material could be deposited on a Si(111) wafer. This material should have a 2DEG surface state in the band gap of Si. As a material, Cu might be a candidate. In addition, CO molecules could be used as potential barriers for the 2DEG. It has been proven that CO can be reliably manipulated on Cu(111) [5].

Lastly, alternatives to a system in which a semi-conductor is covered by another material with a 2DEG in the band gap, can be considered. For instance, InAs which is a semi-conductor with a 2DEG surface state in its own band gap [41].

# 7 Acknowledgements

The last five months have been an immense learning experience for me. Handling the STM and manipulating single atoms in the basement of the Ornstein Laboratory at Utrecht University, truly felt as a privilege. I am very grateful that I can conclude my bachelor's degrees in both physics and chemistry with this thesis project. I would like to thank all who have contributed in making this project happen.

First and foremost, my daily supervisor *Rian Ligthart*. Thank you for teaching me how to control the STM (and manipulate single atoms!) and many other things about conducting experimental research. Furthermore, I would like to thank my project supervisor *Ingmar Swart* for giving me the opportunity to do this project. Also, I want to thank *Jan Cuperus* for always being eager to help me with quick questions about anything. Finally, I would like to express my appreciation for the nice atmosphere in the CMI group, Team Kelder in particular, and the table football matches we played.

# References

[1] A. Trabesinger. Quantum simulation. *Nature Physics*, pages 1745–2481, 4 2012.

[2] G. Binnig and H. Rohrer. Scanning tunneling microscopy. *Surface Science*, 126(1):236–244, 1983.

[3] NobelPrize.org. Press release, 10 1986. Accessed 7 June 2021.

[4] A. A. Khajetoorians, D. Wegner, A. F. Otte, and I. Swart. Designer quantum states of matter created atom-by-atom. *arXiv*, pages 1–23, 2019.

[5] M. R. Slot. *Patterning atomic flatland: Electronic lattices crafted atom by atom.* PhD thesis, Utrecht University, 2019.

[6] M. R. Slot, T. S. Gardenier, P. H. Jacobse, G. C.P. Van Miert, S. N. Kempkes, S. J.M. Zevenhuizen, C. M. Smith, D. Vanmaekelbergh, and I. Swart. Experimental realization and characterization of an electronic Lieb lattice. *Nature Physics*, 13(7):672–676, 2017.

[7] K. K. Gomes, W. Mar, W. Ko, F. Guinea, and H. C. Manoharan. Designer Dirac fermions and topological phases in molecular graphene. *Nature*, 483(7389):306–310, 2012.

[8] S. E. Freeney, S. T. P. Borman, J. W. Harteveld, and I. Swart. Coupling quantum corrals to form artificial molecules. *SciPost Physics*, 9(6):1–18, 2020.

[9] S. N. Kempkes, M. R. Slot, S. E. Freeney, S. J.M. Zevenhuizen, D. Vanmaekelbergh, I. Swart, and C. Morais Smith. Design and characterization of electrons in a fractal geometry. *Nature Physics*, 15(2):127–131, 2019.

[10] J. Girovsky, J. L. Lado, F. E. Kalff, E. Fahrenfort, L. J.J.M. Peters, J. Fernández-Rossier, and A. F. Otte. Emergence of quasiparticle Bloch states in artificial crystals crafted atom-by-atom. *arXiv*, 020:1–12, 2017.

[11] K. F. Braun and K. H. Rieder. Engineering Electronic Lifetimes in Artificial Atomic Structures. *Physical Review Letters*, 88(9):4, 2002.

[12] J. Kliewer, R. Berndt, and S. Crampin. Scanning tunnelling spectroscopy of electron resonators. *New Journal of Physics*, 3, 2001.

[13] G. Meyer, L. Bartels, and K.-H. Rieder. Atom manipulation with the scanning tunneling microscope: nanostructuring and femtochemistry. *Superlattices and Microstructures*, 25(1):463–471, 1999.

[14] J. Li, W.-D. Schneider, R. Berndt, O. R. Bryant, and S. Crampin. Surface-state lifetime measured by scanning tunneling spectroscopy. *Phys. Rev. Lett.*, 81:4464–4467, Nov 1998.

[15] W. Bludau, A. Onton, and W. Heinke. Temperature dependence of the band gap of silicon. *Journal of Applied Physics*, 45:1846–1848, 4 1974.

[16] K. Sawa, Y. Aoki, and H. Hirayama. Thickness dependence of shockley-type surface states of Ag(111) ultrathin films on Si(111)7 × 7 substrates. *Phys. Rev. B*, 80:035428, Jul 2009.

[17] K. F. Braun. PhD thesis, Freie Universität Berlin, 2001.

[18] G. Chang-Zhi, K.F. Braun, and K.H. Rieder. Single atomic manipulation and writing with scanning tunnelling microscopy at low temperatures. *Chinese Physics*, 2002.

[19] K. Bian, C. Gerber, A. J. Heinrich, D. J. Müller, S. Scheuring, and Y. Jiang. Scanning probe microscopy. *Nature Reviews Methods Primers*, 2021.

[20] G. Hörmandinger. Imaging of the Cu(111) surface state in scanning tunneling microscopy. *Phys. Rev. B*, 49:13897–13905, May 1994.

[21] M. van Riggelen. Exploring In on InAs(111)a as a platform for quantum simulation. Bachelor's thesis, Utrecht University, 2020.

[22] G. Meyer, S. Zöphel, and K. H. Rieder. Manipulation of atoms and molecules with a low temperature scanning tunneling microscope. *Appl. Phys. A*, 564(A 63):557–564, 1996.

[23] M. F. Crommie, C. P. Lutz, and D. M. Eigler. Confinement of electrons to quantum corrals on a metal surface. *Science*, 262(5131):218–220, 1993.

[24] G. Binnig and H. Rohrer. In touch with atoms. In Bederson B., editor, *More Things in Heaven and Earth.* Springer, New York, 1999.

[25] W. Shockley. On the surface states associated with a periodic potential. *Phys. Rev.*, 56:317–323, Aug 1939.

[26] I. Tamm. On the possible bound states of electrons on a crystal surface. *Phys. Z. Sowjetunion*, 1:733–735, 1932.

[27] The shapes of atomic orbitals, 2020. https://chem.libretexts.org/@go/page/52808 (Accessed 9 June 2021).

[28] R. W. Robinett. Visualizing the solutions for the circular infinite well in quantum and classical mechanics. *American Journal of Physics*, 64(4):440–446, 1996.

[29] G. A. Fiete and E. J. Heller. Colloquium: Theory of quantum corrals and quantum mirages. *Rev. Mod. Phys.*, 75:933–948, Jul 2003.

[30] R. A. M. Ligthart. Artificial electronic lattices in a magnetic field. Master's thesis, Utrecht University, 2019.

[31] W. Mönch. On the correlation of geometrical structure and electronic properties at clean semiconductor surfaces. *Surface Science*, 63:79–95, 1977.

[32] H. Aizawa, M. Tsukada, N. Sato, and S. Hasegawa. Asymmetric structure of the Si(111)-$\sqrt{3} \times \sqrt{3}$-Ag surface. *Surface Science*, 429:0–5, 1999.

[33] N. Sato, T. Nagao, and S. Hasegawa. Electron standing waves on the Si(111)-$\sqrt{3}\times\sqrt{3}$-Ag surface. *Physical Review B - Condensed Matter and Materials Physics*, 59(3):2035–2039, 1999.

[34] F. Reinert, G. Nicolay, S. Schmidt, D. Ehm, and S. Hüfner. Direct measurements of the l-gap surface states on the (111) face of noble metals by photoelectron spectroscopy. *Phys. Rev. B*, 63:115415, Mar 2001.

[35] J.A. Venables, J. Derrien, and A.P. Janssen. Direct observation of the nucleation and growth modes of Ag/Si(111). *Surface Science*, 95(2):411–430, 1980.

[36] L. Gavioli, K. R. Kimberlin, M. C. Tringides, J. F. Wendelken, and Z. Zhang. Novel growth of ag islands on Si(111): Plateaus with a singular height. *Phys. Rev. Lett.*, 82:129–132, Jan 1999.

[37] D. Nečas and P. Klapetek. Gwyddion: an open-source software for SPM data analysis. *Central European Journal of Physics*, 10:181–188, 2012.

[38] R. A. M. Ligthart and J. P. Coperus. Kelder package, 2021. [python package].

[39] R. A. M. Ligthart, I. Swart, and S. J. M. Zevenhuizen. Muffin tin, 2021. [python package].

[40] L. Bürgi, L. Petersen, H. Brune, and K. Kern. Noble metal surface states: deviations from parabolic dispersion. *Surface Science*, 447(1):L157–L161, 2000.

[41] L. Ö. Olsson, C. B. M. Andersson, M. C. Håkansson, J. Kanski, L. Ilver, and U. O. Karlsson. Charge accumulation at InAs surfaces. *Phys. Rev. Lett.*, 76:3626–3629, May 1996.
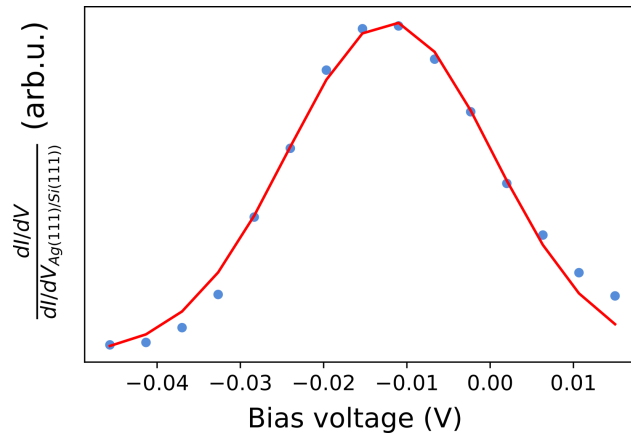
# Appendix: Fitting examples



**Figure 9:** Part of the background divided $dI/dV$ spectrum taken at the centre of corral 1 (blue dots, see section 4.2). The $dI/dV$ data shown in this figure were used to fit a Gaussian function (red solid line).
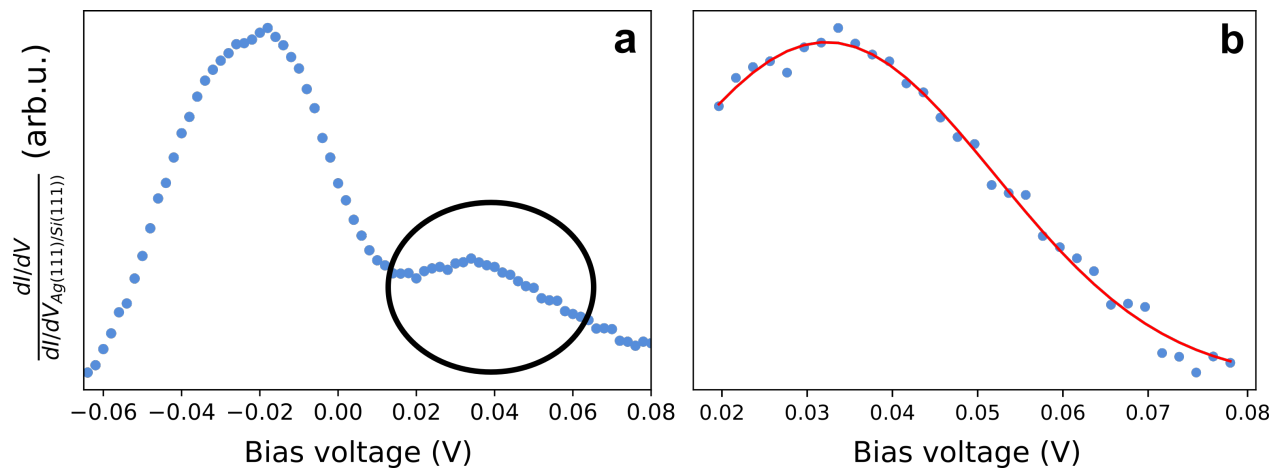


**Figure 10:** **(a)** Part of the background divided $dI/dV$ spectrum taken at the centre of the left corral in the adjusted dimer (blue dots, see section 4.3.2). Two overlapping peaks peaks are observed. Due to the overlap, a Gaussian function could only be fitted to part of each peak. The encircled peak is enlarged in (b). **(b)** The data points of the encircled peak in (a) which were used to fit a Gaussian function, the red solid line.